

Crystallinity of Silicon Nanoparticles: Direct Influence on the Electrochemical Performance of Lithium Ion Battery Anodes

Asbjørn Ulvestad,^{*[a]} Anita H. Reksten,^[a, b] Hanne F. Andersen,^[a] Patricia A. Carvalho,^[c] Ingvild J. T. Jensen,^[c] Marius U. Nagell,^[a] Jan Petter Mæhlen,^[a] Martin Kirkengen,^[a, d] and Alexey Y. Kopusov^{*[a, e]}

The use of silicon (Si) in the form of nanoparticles is one of the most promising routes for boosting the capacity of modern Li-ion batteries. Many parameters influence the performance of Si making the comparison of materials complicated. The present work demonstrates a direct comparison of Si nanoparticles with amorphous and crystalline structures prepared through the same chemistry with the same particle size and morphology. The amorphous Si nanoparticles with an average diameter of 100 nm were synthesized through silane pyrolysis, and their crystalline analogues were obtained through subsequent annealing not altering size or morphology of the nanoparticles. Such direct comparison allows evaluation of the specific impact of crystallinity on the material's performance. From electrochemical analysis of these materials, the electrodes prepared from amorphous nanoparticles were found to exhibit improved cycle life compared to electrodes prepared from crystalline nanoparticles when the delithiation capacity of the anode was limited to 1000 mAh/g_{Si}.

Rechargeable Li-ion batteries (LIBs) offer a great energy storage solution for clean transportation, local energy storage systems, portable power and electronic devices.^[1,2] However, the increasing demands in such applications require new materials which can deliver high energy densities, higher capacities and longer cycle life compared to the present state-of-the-art. The high theoretical gravimetric energy storage capacity (3572 mAh/g for Li₁₅Si₄ phase) and theoretical volumetric energy storage capacity (2081 mAh/cm³) of silicon (Si) has made it an attractive anode material for LIBs to replace the commercial anode material-graphite.^[3] However, Si-based anodes generally exhibit rapid degradation during cycling, partly due to fracturing of active material caused by the large volume changes occurring during lithiation and delithiation.^[4,5] The cracking causes delamination and loss of adhesion between the anode material and the current collector and destroys the conductive network within the electrode, increasing the impedance of the electrode.^[6] Wetjen et al. has also reported that Si particles gradually transform into a nanoporous Si network during cycling.^[7] These processes continuously generate fresh surfaces which become exposed to the electrolyte resulting in the formation of a solid-electrolyte interphase (SEI) which will continue to grow as long as new surfaces are exposed to electrolyte.^[8] Despite the important function of the SEI layer in passivating the active material surface from electrolyte decomposition, its constant formation results in continuous consumption of lithium and electrolyte which are of limited supply in the cell.^[9] This process represents a primary failure mechanism of the Si-based anodes.^[10] To overcome this challenge, the use of nanoparticles was introduced to minimize the stresses caused by volumetric changes, thus preventing further fracturing, and by that mitigate the degradation. However, even at the nano-scale the electrode is therefore still prone to the surface-centred degradation mechanisms.^[11]

Two types of Si nanoparticles have been separately evaluated in the literature – crystalline and amorphous, characterized by different critical size of the particles – a maximum particles size allowing to avoid particle' cracking during lithiation.^[8,12] In addition, multiple strategies have been suggested to improve the stability of Si nanoparticles mostly focused on the crystalline material due to its availability. Such modifications include various coatings, yolk-shell structures^[13,14] and growth of the oxide.^[15,16] Overall, a wide variety of chemical


[a] Dr. A. Ulvestad, Dr. A. H. Reksten, Dr. H. F. Andersen, M. U. Nagell, Dr. J. P. Mæhlen, Dr. M. Kirkengen, Dr. A. Y. Kopusov
Department of Battery Technology
Institute for Energy Technology (IFE)
Instituttveien 18, 2007 Kjeller (Norway)
E-mail: Asbjorn.Ulvestad@ife.no
alexey.kopusov@kjemi.uio.no


[b] Dr. A. H. Reksten
Present address:
SINTEF Industry
Forskningsveien 1, 0373 Oslo (Norway)

[c] Dr. P. A. Carvalho, Dr. I. J. T. Jensen
SINTEF Materials Physics
Forskningsveien 1, 0373 Oslo (Norway)

[d] Dr. M. Kirkengen
Present address:
Cenate AS
Rakkestadveien 1, 1814 Askim (Norway)

[e] Dr. A. Y. Kopusov
Centre for Materials Science and Nanotechnology (SMN)
Department of Chemistry
University of Oslo
P.O. Box 1033, Blindern, 0315 Oslo (Norway)

 Supporting information for this article is available on the WWW under <https://doi.org/10.1002/celec.202001108>

 © 2020 The Authors. ChemElectroChem published by Wiley-VCH GmbH. This is an open access article under the terms of the Creative Commons Attribution License, which permits use, distribution and reproduction in any medium, provided the original work is properly cited.

modifications and strategies have been demonstrated on different Si materials to improve their cyclability.^[17–20] However, different sources of Si materials, variations in particle size and particle size distributions, crystallinity, morphology differences between the reported materials limit the direct comparability of electrochemical performances. In the present work we provide a direct comparison of the pristine amorphous and crystalline Si nanoparticles of the same size and morphology in view of their electrochemical performance in the electrodes of LIBs.

For the present work the amorphous Si nanoparticles (a-Si NPs) were prepared through silane pyrolysis – a convenient and scalable process which allows the growth of spherically shaped Si nanoparticles in the gas phase.^[21] The pyrolysis led to a formation of Si NPs in a form of aggregates with a primary particle size averaging at 100 nm (Figure S1 in supporting information). Crystallization of the NPs was performed by annealing the materials at 1000 °C in a tube furnace under argon atmosphere. Such annealing resulted in the formation of crystalline material (c-Si_{Ar} NPs), the crystallinity of which was confirmed by X-ray diffraction (Figure S2 in supporting information). A high resolution TEM (HRTEM) image of c-Si_{Ar} NP is shown on Figure 1a, additionally confirming the crystal structure. Importantly, the morphology of the particles has been preserved through the crystallization process. The elemental composition of the NPs was confirmed by the elemental analysis demonstrating the loss of residual hydrogen from synthesis after thermal treatment. The surface composition of a-Si and c-Si_{Ar} was characterized by XPS as shown on Figure 1b (survey spectra are shown in Figure S3 with the summary of analysis listed in Table S1 of supporting information). A few major chemical changes are noticeable when analysing the differences between the materials before and after crystallization. Specifically, the XPS analysis revealed the changes of elemental composition at the surface of particles after crystallization. As prepared, a-Si contains approximately 3% of oxygen by weight due to formation of native oxide. When crystallization

is conducted in inert atmosphere, the total amount of oxygen does not change, as it was confirmed by the elemental analysis determined from pyrolysis method (Table S2, supporting information). However, XPS analysis demonstrated the changes in the ratio of silicon/oxygen at the surface after the crystallization was completed (increased oxygen content). We believe such surface changes are caused by the redistribution of oxygen within surface oxide layer during crystallization, where the formation of c-Si_{Ar} resulted in abrupt interface between the SiO_x and Si. The distribution of oxygen was additionally confirmed through TEM analysis combined with EDS mapping (shown on Figure S4 of supporting information).

Therefore, to better separate the changes in the electrochemical performance occurring due to the crystallization effects from the formation of the distinct oxide shell, a separate sample was prepared by annealing at the same temperature, but in the presence of air (c-Si_O NPs). As expected, such treatment resulted in increased amount of oxygen at the surface of the particles (Figure 1 b). Noteworthy, the pristine samples contained small amount of hydrogen embedded in the structure, originating from the preparation method; that residual hydrogen was removed by the heat treatment for c-Si_{Ar} and c-Si_O. Interestingly, some monocrystalline particles of Si were observed in TEM after annealing, which is most likely due to the small size of nanoparticles and the high temperature used during crystallization process (1000 °C), which was considerably higher than the crystallization temperature of Si. Owing to the low sampling of TEM analysis, this is not necessarily representative of the full sample, and it is not ruled out that polycrystalline particles were also formed, as have been previously observed.^[22]

To reveal the effect of crystallinity on nanoparticle's electrochemical performance the resulting materials have been evaluated as electrode materials for LIBs. 50% of Si by weight has been used for electrode fabrication to yield approximately 0.8 mg/cm² loading of Si active material using carboxymethyl cellulose (CMC) as a binder. The electrodes were tested by galvanostatic cycling in a half cell configuration with lithium foil as a counter electrode using LiPF₆-based (1 M) electrolyte in ethylene carbonate/propylene carbonate/dimethyl carbonate mixture (EC:PC:DMC 1:1:3) with 1 wt % vinylene carbonate (VC) and 5 wt % fluoroethylene carbonate (FEC) as additives.^[23] The testing was performed under unlimited capacity conditions (i.e. the active material is utilized to its full lithiation and delithiation capacity between voltage cut-offs of 0.05 V and 1 V vs Li/Li⁺) and under limited capacity conditions, where the delithiation capacity was limited to 1000 mAh/g_{Si}. Cycling under such conditions has been reported to significantly extend the lifetime of the electrodes attributed to the reduced stress applied to the Si nanoparticles.^[24] In addition, such conditions are representative for a typical over dimensioned and prelithiated anode working in a full cell, when the depth of delithiation of the anode is limited by the cathode capacity.^[25] The comparison of representative examples of cycling capacities for the electrodes fabricated from different samples of Si and cycled at either full or limited capacity is shown on Figure 2.

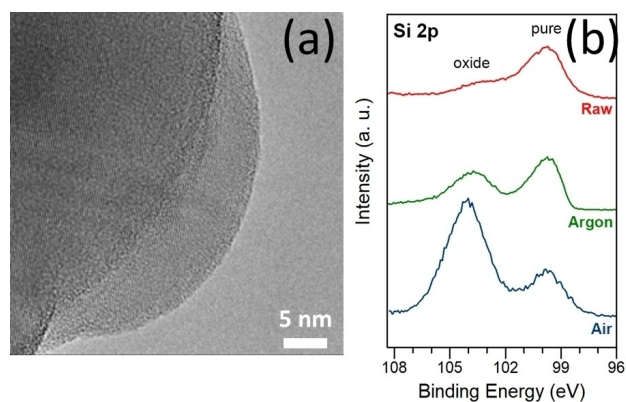


Figure 1. (a) TEM image of Si particles crystallized in inert atmosphere, (b) XPS spectra of Si samples, showing the increase of silicon oxide from a-Si (top) to c-Si_{Ar} (middle) and c-Si_{Ox} (bottom). The intensities have been normalized to the peak maximum of the pure Si component to facilitate comparison. Some peak broadening and shifts to higher binding energy can be observed in the oxidized samples due to challenging charge neutralisation conditions.

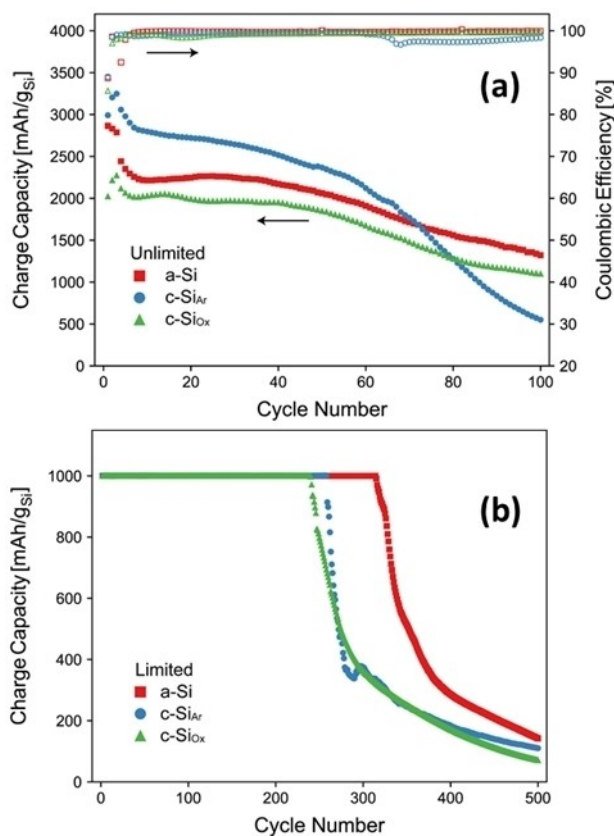


Figure 2. Representative examples of charge/delithiation capacities (including formation cycles) for 3 types of Si (pristine, annealed in Ar and annealed in air) and cycled under (a) full capacity of Si, (b) capacity limited to 1000 mAh/g_{Si}.

(The charge/discharge curves are shown on Figure S5 of Supporting information.)

Cycled at full capacity, a-Si and c-Si_{Ar} demonstrated high capacity around 3000 mAh/g_{Si}, which starts to decline with increased number of cycles, as is typically expected for Si-based anodes.^[26] The capacity fade of the crystalline sample is somewhat faster than for the amorphous equivalent. However, due to the higher capacity of the crystalline material after the formation cycles, the capacity utilization is also higher, which could very well be the cause of the accelerated degradation and testing under such condition therefore does not directly allow elucidation of any benefits of the crystal or amorphous structure of Si NPs. As was expected, the material annealed in the presence of air demonstrates substantially lower capacity due to the presence of substantial amount of oxide. The similar Coulombic efficiencies (which could be correlated with the chemical composition) for a-Si and c-Si_{Ar} indicates a similar amount of total oxygen in the particles, in agreement with the elemental analysis (Table S2 in supporting information).^[16]

Relative to cycling at full capacity, cycling with the capacity limited to 1000 mAh/g_{Si}, substantially extends the lifetime of all electrode types.^[27] Cycling under such conditions leaves part of the material intact, keeping “rest-capacity” which is being utilized through further cycling as Si degrades. When the

accumulated degradation surpasses the theoretical rest capacity (ca 2600 Ah/g_{Si}) it causes a rapid capacity fade after ca 270 and 330 cycles for c-Si electrodes and a-Si electrodes, respectively. These cycling conditions also demonstrate the benefits of using a-Si, as anodes prepared from such material last approximately 50 cycles longer than their crystalline counterparts (c-Si_{Ar} and c-Si_{Ox}).

While a-Si can be lithiated directly, c-Si first needs to undergo an amorphization to allow for complete lithiation, after which both types of the particles are amorphous.^[28] For c-Si the lithiation is known to proceed primarily in the $\langle 110 \rangle$ direction,^[5] resulting in an additional isotropic stress. Therefore, it is reasonable to assume that the initial lithiation involves higher stress for a-Si than that for c-Si and is more damaging to the particles' structure, thus, having a temporarily increased degradation, but that this disadvantage is reduced after the initial lithiation. These cycling results show, however, that there is a prolonged effect of this initial difference which is maintained long after both particle types are assumed to have become amorphous. It is important to note that the particles studied herein have the sizes below the critical size determined for both crystalline and amorphous Si.^[8,12]

The observed differences are, therefore, not expected to be related to particle fracturing, but more likely to the gradual change from particles to porous networks of nanometer-sized branches, as has been reported by Wetjen et al.^[7] Similar changes in Si nanowires have been connected to nano-void formation by Si vacancy aggregation along the interface between the lithiated and delithiated parts of the material during fast lithium extraction.^[29] While not sufficient to fracture the particles, the increased tensile hoop stress in the c-Si particle surface resulting from the two phase lithiation^[8,12] is hypothesized to exacerbate this nanopore formation, thus accelerating the further degradation, which was observed for c-Si_{Ar} and c-Si_{Ox}.

To gain further insight into the improved performance of the a-Si, a differential capacity analysis has been performed on the limited capacity cycling data of the a-Si and c-Si_{Ar} samples, as seen in Figure 3. The inset shows the first cycle of the two sample types clearly illustrating that the lithiation profile of the a-Si is substantially different from dQ/dV profile measured for the crystalline samples. This is primarily seen by a higher lithiation voltage for the amorphous sample, while the lithiation of the crystallized samples occurs at a lower voltage.^[30] The reason for the differences is that c-Si need to go through the activation barrier of the previously mentioned crystalline to amorphous transformation taking place during the initial lithiation, while a-Si is exempt from this.^[28] That also results in different lithiation mechanisms for c-Si and a-Si^[12,31–33] ultimately resulting in different lifetimes of electrodes tested under identical conditions. In the continued cycling, the most prominent differences are the shift of the first lithiation peak (the peak around 0.2 V, corresponding to the formation of amorphous Li_xSi (x~2) phase) to lower voltages and the subsequent shift of the delithiation end-voltage to higher potentials.^[34]

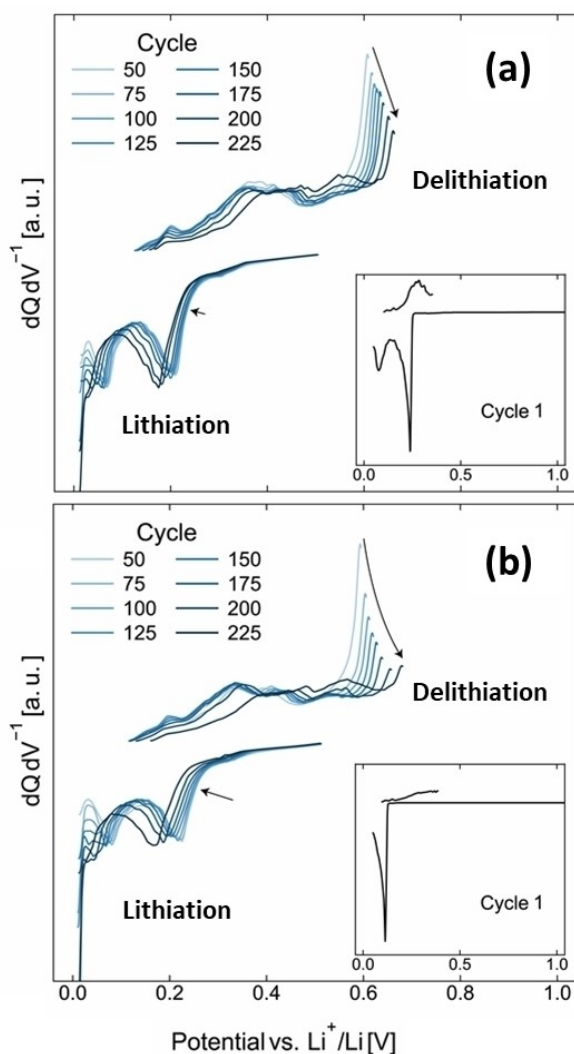


Figure 3. Differential capacity analysis (dQ/dV) for the a-Si (top panel) and c-Si_{Ar} (bottom panel) samples at cycles 50–225 shown with 25 cycles interval. The insets show the 1-st cycle for each type of Si.

The latter shows that the lithiation resistance of the electrode increases faster in the c-Si_{Ar} electrode than in the a-Si electrode, indicating an increased degree of electrode densification and related loss of ionic conductivity in the electrode – common signs of degradation for Si-based electrodes.^[35] The same conductivity loss also partially explains the larger shift of the delithiation end voltage. However, this is also related to an increased utilization of the electrode capacity: as the actual electrode capacity gradually degrades towards the capacity limit, the end-voltage increases towards the 1 V cut-off potential. The larger shift of the c-Si_{Ar} electrode shows that the back-ground degradation of the c-Si_{Ar} is faster than a-Si, notably under the same nominal capacity utilization. This eventually results in the shorter cycle life of c-Si_{Ar}-based electrode than the a-Si-based electrode, as seen in Figure 3 (bottom panel). (Additional differential capacity data is provided in Supporting Information Figures S6 and S7).

In conclusion, the nanoparticles of amorphous and crystalline Si with the same particle size distribution and morphology were compared in terms of their performance in the anodes of LIBs. Cycling at limited capacity unambiguously confirmed the benefits of the amorphous structure which allows to gain a longer lifetime of the electrode compared to the crystalline counterparts. The shorter lifetime of the crystalline silicon is attributed to the initial structural stress caused by the initial lithiation.

Acknowledgements

Funding support was provided by the Research Council of Norway through the ENERGIX Project No. 243802 and No. 280985. This work was performed within MoZEEs, a Norwegian Centre for Environment-friendly Energy Research (FME), co-sponsored by the Research Council of Norway (project number 257653) and 40 partners from research, industry and public sector. The authors kindly thank Dr. V. A. Yartys for fruitful discussions of the results and Dynatec AS for assistance with the preparation of a-Si. The Research Council of Norway is acknowledged for the support to the Norwegian Center for Transmission Electron Microscopy, NORTEM (project 197405/F50).

Conflict of Interest

The authors declare no conflict of interest.

Keywords: anode materials · limited capacity · lithium ion batteries · nanoparticles · silicon

- [1] N. Nitta, F. Wu, J. T. Lee, G. Yushin, *Mater. Today* **2015**, *18*, 252–264.
- [2] J. M. Tarascon, M. Armand, *Nature* **2001**, *414*, 359–367.
- [3] N. Delpuech, D. Mazouzi, N. Dupré, P. Moreau, M. Cerbelaud, J. S. Bridel, J. C. Badot, E. De Vito, D. Guyomard, B. Lestriez, B. Humbert, *J. Phys. Chem. C* **2014**, *118*, 17318–17331.
- [4] M. N. Obrovac, L. Christensen, *Electrochem. Solid-State Lett.* **2004**, *7*, A93.
- [5] M. T. McDowell, S. W. Lee, W. D. Nix, Y. Cui, *Adv. Mater.* **2013**, *25*, 4966–4985.
- [6] K. Feng, M. Li, W. Liu, A. G. Kashkooli, X. Xiao, M. Cai, Z. Chen, *Small* **2018**, *14*, 1702737.
- [7] M. Wetjen, S. Solchenbach, D. Pritzl, J. Hou, V. Tileli, H. A. Gasteiger, *J. Electrochem. Soc.* **2018**, *165*, A1503–A1514.
- [8] X. H. Liu, L. Zhong, S. Huang, S. X. Mao, T. Zhu, J. Y. Huang, *ACS Nano* **2012**, *6*, 1522–1531.
- [9] H. Wu, G. Chan, J. W. Choi, I. Ryu, Y. Yao, M. T. McDowell, S. W. Lee, A. Jackson, Y. Yang, L. Hu, Y. Cui, *Nat. Nanotechnol.* **2012**, *7*, 310–315.
- [10] M. Nie, D. P. Abraham, Y. Chen, A. Bose, B. L. Lucht, *J. Phys. Chem. C* **2013**, *117*, 13403–13412.
- [11] H. Li, *Electrochem. Solid-State Lett.* **1999**, *2*, 547.
- [12] M. T. McDowell, S. W. Lee, J. T. Harris, B. A. Korgel, C. Wang, W. D. Nix, Y. Cui, *Nano Lett.* **2013**, *13*, 758–764.
- [13] L. Zhang, C. Wang, Y. Dou, N. Cheng, D. Cui, Y. Du, P. Liu, M. Al-Mamun, S. Zhang, H. Zhao, *Angew. Chem.* **2019**, *131*, 8916–8920.
- [14] N. Liu, H. Wu, M. T. McDowell, Y. Yao, C. Wang, Y. Cui, *Nano Lett.* **2012**, *12*, 3315–3321.
- [15] M. T. McDowell, S. W. Lee, I. Ryu, H. Wu, W. D. Nix, J. W. Choi, Y. Cui, *Nano Lett.* **2011**, *11*, 4018–4025.
- [16] Y. Cao, J. C. Bennett, R. A. Dunlap, M. N. Obrovac, *Chem. Mater.* **2018**, *30*, 7418–7422.

- [17] P. Li, G. Zhao, X. Zheng, X. Xu, C. Yao, W. Sun, S. X. Dou, *Energy Storage Mater.* **2018**, *15*, 422–446.
- [18] M. Ashuri, Q. He, L. L. Shaw, *Nanoscale* **2016**, *8*, 74–103.
- [19] G. G. Eshetu, E. Figgemeier, *ChemSusChem* **2019**, *12*, 2515–2539.
- [20] X. Zuo, J. Zhu, P. Müller-Buschbaum, Y.-J. Cheng, *Nano Energy* **2017**, *31*, 113–143.
- [21] H. F. Andersen, W. Filtvedt, J. P. Mæhlen, T. T. Mongstad, M. Kirkengen, A. Holt, *ECS Trans.* **2014**, *62*, 97–105.
- [22] H. Hofmeister, J. Dutta, H. Hofmann, *Phys. Rev. B* **1996**, *54*, 2856–2862.
- [23] L. C. Loaiza, E. Salager, N. Louvain, A. Boulaoued, A. Iadecola, P. Johansson, L. Stievano, V. Seznec, L. Monconduit, *J. Mater. Chem. A* **2017**, *5*, 12462–12473.
- [24] M. N. Obrovac, V. L. Chevrier, *Chem. Rev.* **2014**, *114*, 11444–11502.
- [25] G. Gabrielli, M. Marinaro, M. Mancini, P. Axmann, M. Wohlfahrt-Mehrens, *J. Power Sources* **2017**, *351*, 35–44.
- [26] S. Y. Lai, K. D. Knudsen, B. T. Sejersted, A. Ulvestad, J. P. Mæhlen, A. Y. Kozosov, *ACS Appl. Mater. Interfaces* **2019**, *2*, 3220–3227.
- [27] H. F. Andersen, C. E. L. Foss, J. Voje, R. Tronstad, T. Mokkalbost, P. E. Vullum, A. Ulvestad, M. Kirkengen, J. P. Mæhlen, *Sci. Rep.* **2019**, *9*, 14814.
- [28] J. Li, J. R. Dahn, *J. Electrochem. Soc.* **2007**, *154*, A156.
- [29] J. Zhu, M. Guo, Y. Liu, X. Shi, F. Fan, M. Gu, H. Yang, *ACS Appl. Mater. Interfaces* **2019**, *11*, 17313–17320.
- [30] W.-R. Liu, Z.-Z. Guo, W.-S. Young, D.-T. Shieh, H.-C. Wu, M.-H. Yang, N.-L. Wu, *J. Power Sources* **2005**, *140*, 139–144.
- [31] B. Key, R. Bhattacharyya, M. Morcrette, V. Seznéc, J.-M. Tarascon, C. P. Grey, *J. Am. Chem. Soc.* **2009**, *131*, 9239–9249.
- [32] X. H. Liu, J. W. Wang, S. Huang, F. Fan, X. Huang, Y. Liu, S. Krylyuk, J. Yoo, S. A. Dayeh, A. V. Davydov, S. X. Mao, S. T. Picraux, S. Zhang, J. Li, T. Zhu, J. Y. Huang, *Nat. Nanotechnol.* **2012**, *7*, 749–756.
- [33] J. W. Wang, Y. He, F. Fan, X. H. Liu, S. Xia, Y. Liu, C. T. Harris, H. Li, J. Y. Huang, S. X. Mao, T. Zhu, *Nano Lett.* **2013**, *13*, 709–715.
- [34] K. Ogata, E. Salager, C. J. Kerr, A. E. Fraser, C. Ducati, A. J. Morris, S. Hofmann, C. P. Grey, *Nat. Commun.* **2014**, *5*, 3217.
- [35] M. Wetjen, D. Pritzl, R. Jung, S. Solchenbach, R. Ghadimi, H. A. Gasteiger, *J. Electrochem. Soc.* **2017**, *164*, A2840–A2852.

Manuscript received: August 21, 2020

Revised manuscript received: October 8, 2020

Accepted manuscript online: October 9, 2020